Binding of SARS-CoV-2 protein ORF9b to mitochondrial translocase TOM70 prevents its interaction with chaperone HSP90

Kehinde S. Ayinde [a, b], Glaucia M.S. Pinheiro [a], Carlos H.I. Ramos [a, *]

[a] Institute of Chemistry, University of Campinas UNICAMP, 13083-970, Campinas, SP, Brazil
[b] Institute of Biology, University of Campinas (UNICAMP), SP, Brazil

ARTICLE INFO

ABSTRACT

The emergence of the COVID-19 pandemic, caused by severe acute respiratory syndrome coronavirus 2 (SARS-CoV-2), remains a great threat to global health. ORF9b, an important accessory protein of SARS-CoV-2, plays a critical role in the viral host interaction, targeting TOM70, a member of the mitochondrial translocase of the outer membrane complex. The assembly between ORF9b and TOM70 is implicated in disrupting mitochondrial antiviral signaling, leading to immune evasion. We describe the expression, purification, and characterization of ORF9b alone or coexpressed with the cytosolic domain of human TOM70 in *E. coli*. ORF9b has 97 residues and was purified as a homodimer with an molecular mass of 22 kDa as determined by SEC-MALS. Circular dichroism experiments showed that Orf9b alone exhibits a random conformation. The ORF9b-TOM70 complex characterized by CD and differential scanning calorimetry showed that the complex is folded and more thermally stable than free TOM70, indicating strong binding. Importantly, protein−protein interaction assays demonstrated that full-length human Hsp90 is capable of binding to free TOM70 but not to the ORF9b-TOM70 complex. To narrow down the nature of this inhibition, the isolated C-terminal domain of Hsp90 was also tested. These results were used to build a model of the mechanism of inhibition, in which ORF9b efficiently targets two sites of interaction between TOM70 and Hsp90. The findings showed that ORF9b complexed with TOM70 prevents the interaction with Hsp90, and this is one major explanation for SARS-CoV-2 evasion of host innate immunity via the inhibition of the interferon activation pathway.

© 2022 Elsevier B.V. and Société Française de Biochimie et Biologie Moléculaire (SFBBM). All rights reserved.

1. Introduction

Human coronaviruses have been periodically emerging over a number of times and have continued to bewilder to humankind by causing a worldwide pandemic. Severe acute respiratory syndrome coronavirus-2 (SARS-CoV-2) causes COVID-19, which is responsible for the ongoing outbreak, and efforts to exploit various viral target proteins for possible cure and therapy continue to remain the topmost research priority today [1]. Although great success has been registered in vaccine production to mitigate the spread of this virus, various challenges, such as the emergence of different strains and mutations, remain a major aspect of concern. Importantly, the ability of this virus to escape the host antiviral defense system and target the humoral immune system, which further results in severe deterioration of the body, has become a major point of focus in attempts to find a lasting cure for the virus [2].

Wang and colleagues [3] reported that the nucleocapsid protein of SARS-CoV-2 could inhibit the key signaling adaptor mitochondrial antiviral-signaling (MAVS) protein, which is activated by RIG-I, limiting the host defense response to the virus. MAVS is an important player in the innate immune response pathways and is a major strategy used by SARS-CoV-2 to evade antiviral immunity [3]. However, other studies confirmed that an accessory protein from SARS-CoV-2, ORF9b, impaired the induction of types I and III interferons (IFNs) by interacting with MAVS assembly, bringing attention to the importance of ORF9b in host antiviral system evasion by the virus [4–6]. SARS-CoV-2 ORF9b is an alternative ORF located within the nucleocapsid (N) gene that codes for a 97 amino acid protein and has similar characteristics to its SARS-CoV homologue (ORF9b, 98 residues, 72.4% similarity). The structure of ORF9b forms a beta sheet-rich homodimer with a hydrophobic cavity in the center that binds lipids [6].

Abbreviations

CD	circular dichroism
DSC	differential scanning calorimetry
Hsp	heat shock protein
Hsp90	90 kDa Hsp
IFN	interferons
IRF3	interferon regulatory factor
MAVS	mitochondria antiviral system
ORF9b	open reading frame 9b
SEC	size exclusion chromatography
SEC-MALS	SEC coupled to multiangle light scattering
TBK	TANK-binding kinase
TOM70	70 kDa mitochondria translocase of outer membrane subunit
TPR	tetratricopeptide repeat

The critical involvement of TOM70 with MAVS in a cascade that produces INF–I leading to an innate immune response specifically to viral RNA is likely the most suitable explanation for the suppression of INF–I by the ORF9b-TOM70 interaction. TOM70 is a member of the translocase of the outer membrane complex that mediates chaperone dependent import of preproteins in the cytosol into the mitochondria [7]. TOM70 contains at least seven tetratricopeptide repeat (TPR) domains in its cytosolic segment. The TPR structure is characterized by the presence of 34 amino acid repeats forming two anti-parallel α-helices separated by a turn, and a triad (TPR clamp domain) has the ability to bind the Hsp90 C-terminal MEEVD motif [8,9]. During viral infection, viral RNA is recognized by the cytosolic helicase RIG-I, which undergoes a conformational change and associates with MAVS, triggering the association of MAVS with TOM70 and initiating the recruitment of Hsp90, where the C-terminal MEEVD motif of Hsp90 binds to the N-terminal TPR domain of TOM70 [10–14]. IRF3 is then phosphorylated by TBK1, which leads to its dissociation from the MAVS complex. Then, phosphorylated IRF3 translocates into the nucleus and promotes the transcription of genes encoding INF–I.

Since TOM70's interaction with the MEEVD motif of Hsp90 via the TPR domain is key for its function in the interferon pathway and induction of apoptosis upon viral infection, we asked whether ORF9b, by binding to the substrate recognition site of TOM70, allosterically inhibits TOM70's interaction with Hsp90. To gather detailed information about the mechanism of inhibition, not only the full-length HSP90 but also its C-terminal domain were studied. This approach proved to be relevant to build a model for the mechanism of inhibition.

2. Experimental procedures

2.1. Recombinant protein production

A codon-optimized ORF9b from SARS-CoV-2 was cloned into pET28a with the insertion of both a poly-histidine tag (His-tag) and a cleavage site for TEV protease. The ORF9b recombinant protein was expressed in *E. coli* BL21(DE3) cells grown in LB media with 30 μg mL^{-1} kanamycin at 37 °C until an Abs$_{600}$ of 0.8 was reached, and the expression was induced with 0.5 mM isopropyl β-D-1-thiogalactopyranoside (IPTG) at 37 °C for 4 h. The cytosolic fragment of TOM70 (UniProtKB - O94826, residues 111–608) cloned into the pPROEX plasmid [7] and ORF9b cloned into pET28a was heat-shock cotransformed into and coexpressed in *E. coli* BL21(DE3) cells at 1 mM IPTG and 37 °C for 4 h, then cells were harvested by centrifugation at 2450 g for 15 min at 4 °C. The pellet was resuspended in 25 mM Tris HCl and 200 mM NaCl, pH 9.0, and incubated with 1 mM PMSF, 30 μg mL^{-1} lysozyme and 5 U of DNAse for 30 min on ice. Cells were lysed using a sonicator and centrifuged at 20,000×*g* for 30 min at 4 °C. Either His-tagged ORF9b or ORF9b-TOM70 complex was purified using 5 mL nickel affinity column HisTrap™ HP (GE Healthcare) equilibrated in buffer A (25 mM Tris HCl, pH 8.0, 200 mM NaCl and 20 mM imidazole) and was eluted with buffer B (25 mM Tris HCl, pH 8.0, 200 mM NaCl and 500 mM imidazole). Proteins were further purified over a Superdex 200 26/60 gel filtration column (GE Healthcare) in GF buffer (25 mM Tris HCl, pH 8.0 and 200 mM NaCl) using a FPLC AKTA system (Amersham Pharmacia Biotech). All purification steps were accessed by SDS–PAGE, and concentration was determined using absorbance at 280 nm by the Edelhock method [15]. Other recombinant proteins used in the study, including full-length human Hsp90 (UniProtKB - P07900), and the C-terminal domain of human Hsp90 (residues 566–732) were expressed and purified as previously reported [9,16].

2.2. Spectroscopy

Circular dichroism (CD) was recorded on a spectropolarimeter J-810 (JASCO) device with a temperature controller (*Peltier Type Control System PFD 4255-jasco*) under constant flow of 10 L min^{-1} N$_2$. Protein samples (5 μM) in 25 mM Tris HCl pH 8.0 and 200 mM NaCl were placed into a 2 mm optical length quartz cuvette. Each obtained spectrum was an average of 16 different readings at 200–260 nm wavelengths measured at 20 nm min^{-1} with a 1 s response time at 20 °C. The results were expressed as the mean residue molar ellipticity, $[\theta]$ [17].

Fluorescence measurements were performed in a spectrofluorimeter (SLM AMINCO-Bowman Series 2 (AB2) (Thermo Fisher, Inc.) at 25 °C using a 1 × 1 cm pathlength cuvette with 10 μM of protein sample in the above buffer. The fluorescence intensity was measured with excitation at 295 nm and emission from 300 to 400 nm.

2.3. Differential scanning calorimetry

Differential scanning calorimetry (DSC) was used to directly measure the thermodynamic parameters using a MicroCal Ultrasensitive VP-DSC apparatus. Protein samples at 20 μM (in buffer 25 mM Tris HCl, pH 8.0 and 200 mM NaCl) were degassed for 30 min before loading into the calorimeter. The scans were performed at scan rates of 60 °C h^{-1}. The data obtained were subtracted from a baseline of buffer against buffer before normalization of the protein concentration and analyzed using Origin® VP-DSC software.

2.4. Pull-down assay

The His-tag of Hsp90 was removed by TEV protease to be used as prey in the pull-down assay, while His-tagged TOM70 and the ORF9b-TOM70 complex were used as bait. The pull-down experiment was performed in GF buffer (25 mM Tris HCl, pH 8.0 and 200 mM NaCl) and conducted at room temperature. Three mL of 20 μM His-tagged TOM70 and ORF9b-TOM70 complex were immobilized in separate experiments into a 5 mL HisTrap™ HP (GE Healthcare) nickel column. Wash with 3 collumn volumes (CV) used the same buffer to ensure that any unbound protein was washed away from the column. Then, 3 mL of 20 μM untagged Hsp90 was injected into the column and incubated for 2 h at 4 °C. After incubation, the column was washed again with 3 CV of buffer A to remove noninteracting proteins. Finally, proteins bound

specifically to the resin of the column and their interacting proteins were eluted with buffer containing 500 mM imidazole. Samples were collected at each step and analyzed by SDS–PAGE.

2.5. Size-exclusion chromatography-multiangle light scattering (SEC-MALS)

Size exclusion chromatography (SEC) coupled with multiangle light scattering (MALS) was used to determine protein molecular mass [18]. This device was set up with a 25 mL column Superdex 200 10/300 GL (GE Healthcare) connected to an ÄKTA pure protein purification system (Amershan Pharmacia Biotech) coupled with a triple light detector miniDAWN TREOS (Wyatt Technologies) and Optilab T-rEX refractive index detector (Wyatt Technologies). Protein mixtures were incubated for 4 h at 4 °C at the same concentration. After incubation, the samples were applied to the SEC-MALS at 25 °C, and sample fractionation was collected and analyzed with 12% SDS–PAGE. Molecular masses were determined by ASTRA (Wyatt Technologies) software. Additionally, characteristic profiles from the chromatogram, molecular mass, and SDS–PAGE were used to evaluate protein–protein interactions.

3. Results and discussion

3.1. ORF9b is purified as a mainly disordered homodimer

Accessory proteins of SARS-CoV-2 are encoded by individual ORFs, such as ORF9b, which is involved in modulating the response to infection [3]. This response triggers a cascade that leads to the production of the antiviral protein interferon and includes the mitochondrial antiviral signaling (MAVS) protein [3]. ORF9b likely disrupts the response by binding to the mitochondrial outer membrane protein TOM70 [3,19]. Thus, a detailed understanding of the mechanism of interaction has great potential to be relevant in the development of therapeutic strategies against COVID-19 [11]. To contribute to such understanding, this investigation aimed to produce, characterize and investigate the interactions of ORF-9b (Fig. 1A) and the cytosolic fraction of human TOM70 (Fig. 1B) by a combination of experimental tools [20].

Purified ORF9b had a molecular mass of 22.0 ± 1.0 kDa, as shown by SEC-MALS (Fig. 2A), confirming the homodimeric assembly of
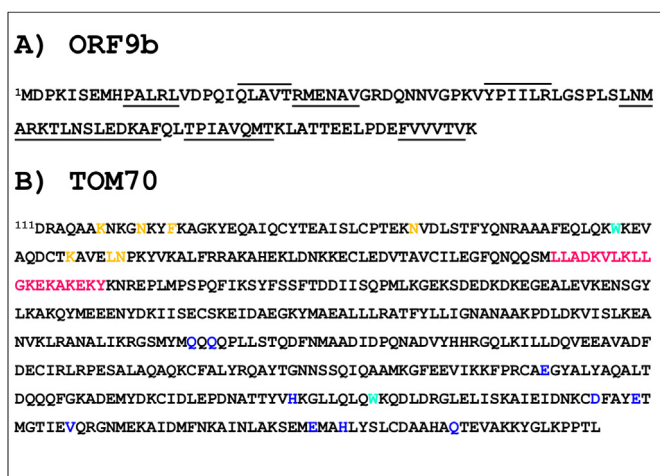

Fig. 1. Amino acid sequences of ORF9b (A) and cytosolic TOM70 (B). A) Secondary structure predicted by PSIPRED: helix, under line; strand/sheet, upper line; coil, no line. **B)** Colors are the same as in Fig. 6. Yellow, residues binding the MEEVD motif of Hsp90; cyan, Trp residues; magenta, residues binding the second binding site of Hsp90; blue, residues binding ORF9b.
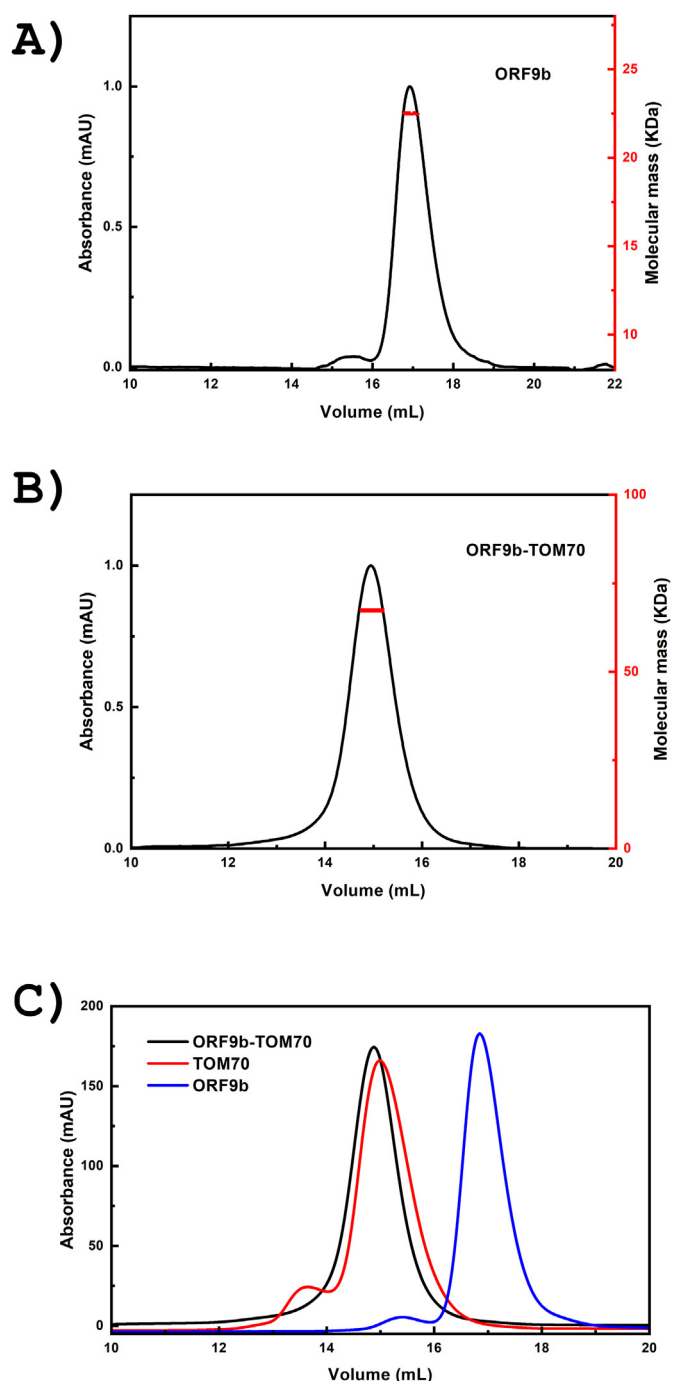

Fig. 2. Molecular mass determination A) ORF9b had a molecular mass of 22.0 ± 1.0 kDa as indicated by SEC-MALS analysis. **B)** ORF9b-TOM70 had a molecular mass of 67.0 ± 1.0 kDa, as indicated by SEC-MALS analysis. **C)** SEC-MALS profiles. Elution is dependent on the molecular mass, and ORF9b-TOM70 was eluted before TOM70 alone, indicating the formation of a complex.

ORF9b since the polypeptide is predicted to be 10.8 kDa from its amino acid sequence (Fig. 1A). A crystal structure of ORF9b from SARS-CoV and SARS-CoV-2 (PDB id: 2CME, 6Z4U) confirmed its homodimeric structure and the existence of a hydrophobic central tunnel for lipid binding [11].

The CD spectrum of ORF9b was characteristic of a disordered polypeptide with a minimum at approximately 206 nm (Fig. 3A). However, several structural characteristics of the ORF9b structure using other techniques, such as electron microscopy and cryo-EM,
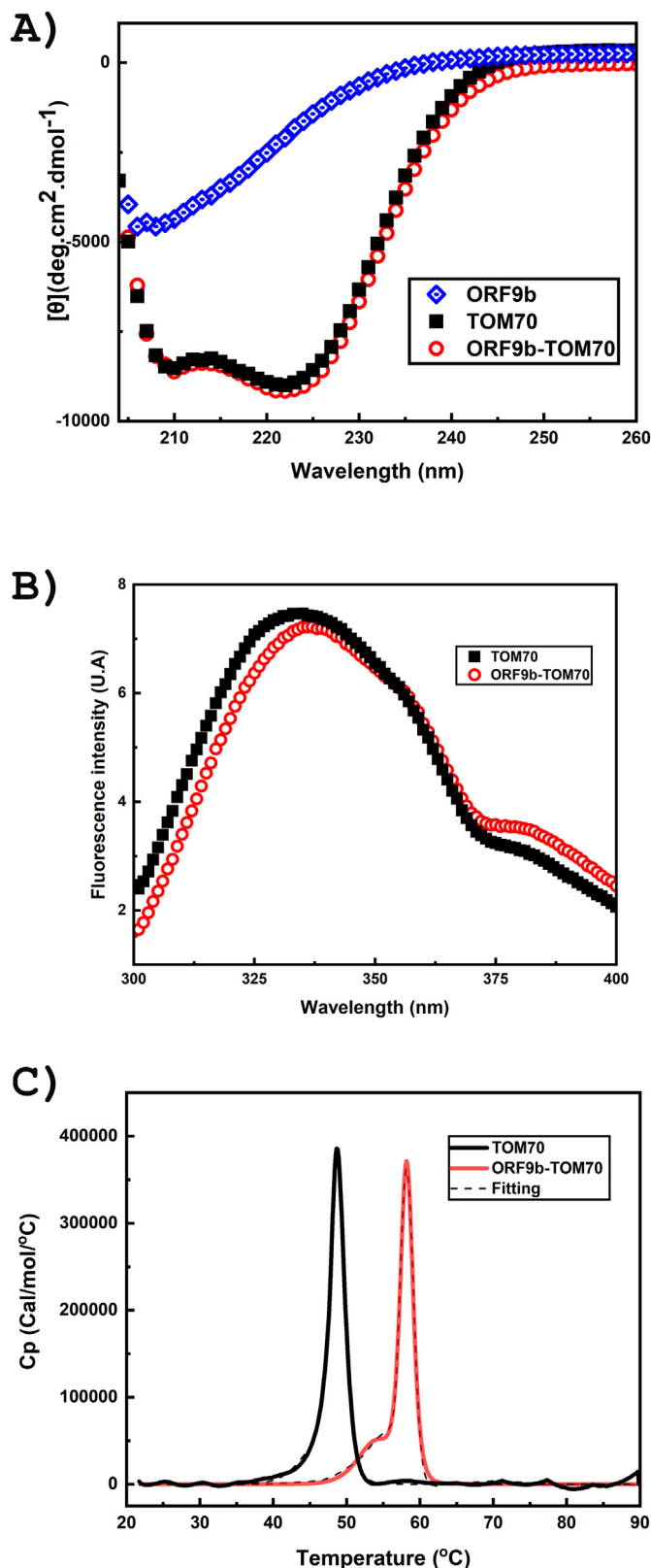
Fig. 3. Characterization of ORF9b and the ORF9b-TOM70 complex. A) Circular dichroism (CD) spectra of SAR-CoV-2 ORF9b, cytosolic human TOM70 and the ORF9b-TOM70 complex. The ORF9b spectrum indicates a predominant random coil conformation. ORF9b-TOM70 and TOM70 α-helical contents do not differ and are approximated 76%. **B)** Emission fluorescence spectra of ORF9b-TOM70 and TOM70 are indistinguishable. TOM70 has two tryptophan residues, while ORF9b has none. **C)** Differential scanning calorimetry profiles of ORF9b-TOM70 and TOM70. T_{m1} and T_{m2}

indicate that ORF9b is a 2-fold symmetric dimer constructed from two adjacent twisted β sheets forming strands contributed by both monomers with highly interlocked architecture reminiscent of a handshake [11]. The CD result revealed that a major part, but not all, of the protein was disordered, which is supported by the analysis of the protein sequence by PSIPRED that confirmed that a large part of the sequence is disordered (underlined in Fig. 1A). More interestingly, ORF9b is believed to belong to the family of proteins referred to as fold switches [21]. Fold-switching proteins remodel their secondary structures and change their functions in response to environmental stimuli. It is likely that the β-sheets that are best used to describe the homodimeric structure of the protein are connected by a large random coil region (PDB; 6Z4U).

3.2. ORF9b binds cytosolic TOM70 to produce a stable complex

Coexpression of ORF9 and TOM70 produced a pure ORF9-TOM70 complex after two stages of purification by affinity and SEC. SEC-MALS showed that the complex had a molecular mass of 67.0 ± 2.0 kDa, indicating that it was formed with one monomer each of ORF9b and TOM70 (Fig. 2B). This is consistent with the two solved structures of the ORF9b-TOM70 complex by cryo-EM [12] and X-ray crystallography [11]. Furthermore, we confirmed the chromatogram of elution fractions of ORF9b-TOM70, TOM70, and ORF9b alone by SEC, which showed a shift in the elution peak of the proteins, confirming the increased molecular mass in the ORF9b-TOM70 complex when compared to TOM70 alone (Fig. 2C).

Likewise, CD was used to determine the secondary structure characteristics of the ORF9b-TOM70 complex, which was compared with TOM70 alone and was indistinguishable inside the error (Fig. 3A). Each spectrum had two minima of approximately −9000 and −8500 deg.cm^2.dmol^{-1} at 222 and 208 nm, respectively, indicating proteins predominantly composed of α-helices, approximately 77% and 76%, respectively, by using methods proposed by Morriset et al. [22] and Greenfield and Fasman [23].

Tryptophan fluorescence is a remarkable tool to investigate local protein conformation because its side chain is sensitive to the polarity of its environment, in a polar environment, as, for instance, solvent exposure, it emits fluorescence with a maximum at approximately 350 nm, which blueshifts in a polar environment, as, for instance, buried in the protein [24]. ORF9b has no Trp residues, while TOM70 has two (Fig. 1), and fluorescence experiments with excitation at 295 nm provide information on whether at least one of the residues was affected by the formation of the complex. The two spectra had similar shapes and intensities (Fig. 3B), indicating no significant conformational changes in the regions in which the Trps are located. The implication of this result is discussed below.

Thermodynamic studies of the complex and comparison with TOM70 alone showed a strikingly more stable ORF9b-TOM70 complex. Thermal stability was investigated by differential scanning calorimetry (DSC), and Fig. 3C shows the heat capacity profile for both TOM70 and ORF9b-TOM70. The shapes of the heat capacity profiles were similar, as they seemed to have a shoulder before a sharp transition. The shoulder is likely due to some oligomeric (maybe dimer) form of TOM70 that was in equilibrium with the monomer (although that was the only form detected by SEC-MALS, i.e., the largely predominant species). Transitions were from 41 to 52 °C for TOM70 alone and from 50 to 61 °C ORF9b-TOM70 (Fig. 3C) and better fitted with two endotherms. T_{m1} and T_{m2} (T_m, temperature at the middle of the transition) of the endotherms of TOM70 alone were 46 and 49 °C, respectively, and T_{m1} and T_{m2} of the

of the TOM70 endotherms were 46 and 49 °C, respectively, and T_{m1} and T_{m2} of the ORF9b-TOM70 endotherms were 54 and 58 °C, respectively.

endotherms of ORF9b-TOM70 were 54 and 58 °C, respectively (Fig. 3C and Table 1). Although thermal-induced unfolding profiles were poorly reversible (data not shown), the T_{m2} values strongly supported the conclusion that TOM70 bound to ORF9-b was more stable than TOM70 alone, indicating that the interaction generates well-packed protein interfaces [25].

3.3. Binding of ORF9b to TOM70 precludes its interaction with Hsp90

To specify whether ORF9b, by binding to TOM70, affects its binding to Hsp90, we employed a pull-down protein—protein interaction approach. In this method, the interaction of Hsp90 with ORF9b-TOM70 or TOM70 was studied by using protein samples consisting of a poly histidine tag, which can specifically bind to the nickel affinity column representing a bait, and thereby incubating them with Hsp90 free of the His tag (cleaved by TEV protease). Hsp90 firmly binds with TOM70, and both were only eluted as a complex only when 500 mM imidazole was used to decrease the affinity of TOM70 to the resins (Fig. 4A). However, Hsp90 failed to bind the ORF9b-TOM70 complex, as was observed from SDS—PAGE analysis (Fig. 3B). In this case, Hsp90 was eluted with wash buffer after incubation.

Analytical gel filtration and SEC-MALS were performed to further study the protein—protein interactions, and the oligomeric states of the full-length Hsp90 and ORF9b-TOM70 complexes showed that they eluted as independent peaks. This shows that both proteins failed to interact upon incubation, and this was evident when the peaks were analyzed by SDS—PAGE (Fig. 5A). To gather more information, this experiment was repeated with Hsp90 treated with 50 mM nonhydrolyzable ATP and ADP (data not shown), and similar independent peaks were observed, showing that Hsp90 failed to bind with the ORF9b-TOM70 complex either in the presence or absence of nucleotides. On the other hand, Fig. 5B shows that Hsp90 and TOM70 were able to produce a complex with the highest peak corresponding to the Hsp90 and TOM70 complex, and this was confirmed by SDS—PAGE. Moreover, SEC-MALS analysis (Fig. 2B) specified a stoichiometric arrangement of one monomer of TOM70 to a dimer of Hsp90 in the complex, a result in agreement with our previously published works that described the binding of TOM70 with Hsp90 [7,9].

The MEEVD motif of Hsp90 specifically binds the cytosolic TPR (tetratricopeptide) clamp of TOM70 [26], and in a previous work, we studied the interaction of the C-terminal domain of Hsp90 (C-Hsp90) with TOM70 and found a second site of interaction [9]. Thus, the interaction of this domain with the ORF9b-TOM70 complex was investigated to add information on the mechanism of inhibition. Fig. 5C shows an analytical gel filtration chromatogram of a mixture of ORF9b-TOM70 and C-Hsp90, and we observed two distinct peaks analyzed by SDS—PAGE, indicating no complex formation, a result similar to that of full-length Hsp90. However, as expected, the mixture of C-Hsp90 with TOM70 alone eluted as a single peak with a molecular mass of ~110 kDa (SEC-MALS analysis not shown), and peaks analyzed by SDS—PAGE showed the two protein bands present in the peak (Fig. 5D), indicating the same stoichiometry arrangement of 2:1 (C-Hsp90:TOM70).

Table 1
Summary of the thermodynamic parameters of TOM70 and ORF9b-TOM70. The uncertainties listed are the standard errors of the mean.

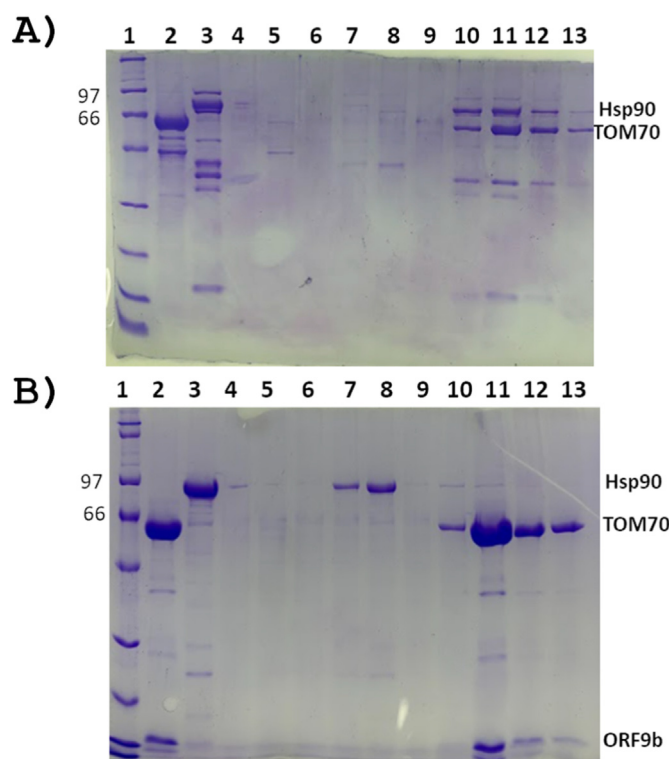| Protein	T_{m1} (°C)	ΔH_1 (kcal/mole/°C)	T_{m2} (°C)	ΔH_2 (kcal/mole/°C)
TOM70	46 ± 1	295 ± 20	49 ± 1	930 ± 60
ORF9b-TOM70	54 ± 1	340 ± 30	58 ± 1	820 ± 50

Fig. 4. Pull-down assay. A) Pull-down assays of TOM70 with full-length Hsp90. The TOM70 His-tagged construct was maintained intact, while Hsp90 with its His-tag was removed by TEV protease. SDS—PAGE analysis of samples at each stage of the experiment is shown. Lanes: 1. Molecular mass marker (Benchmark™ Protein ladder Invitrogen); 2. His-TOM70 (bait control); 3. Hsp90 (prey control); 4. Flow through His-TOM70 (bait); 5—6. Wash with buffer A; 7. Flow through Hsp90; 8—9. Wash with buffer A; 10—13. Elution with buffer B (500 mM imidazole). Flow through of His-TOM70 shows that the protein was bound to the nickel column upon two steps of wash. Flow through of Hsp90 shows that Hsp90 was bound to TOM70 and was not dissociated upon two-step buffer A wash. Elution by buffer B containing imidazole confirmed the presence of His-TOM70 bound to Hsp90. **B)** Pull-down assays of ORF9b-TOM70 with full-length Hsp90. The ORF9b-TOM70 His-tagged construct was maintained intact, while Hsp90 had its His-tag removed by TEV protease. SDS—PAGE analysis of samples at each stage of the experiment is shown. Lanes: 1. Molecular mass marker (Benchmark™ Protein ladder Invitrogen); 2. His-ORF9b-TOM70 (bait control); 3. Hsp90 (prey control); 4. Flow through His-ORF9b-TOM70 (bait); 5—6. Wash with buffer A; 7. Flow through Hsp90 (prey); 8—9. Wash with buffer A; 10—13. Elution with buffer B (500 mM imidazole). Flow through of His-ORF9b-TOM70 shows that the protein was bound to the nickel column upon two steps of wash. Flow through of Hsp90 shows that Hsp90 failed to bind to the complex and was eluted by buffer A wash. Elution by buffer B containing imidazole removed bound protein from the column.

3.4. On the mechanism of inhibition of Hsp90 TOM70 interaction by ORF9b

In a previous study, one of the main experiments utilized to identify the second site of interaction between Hsp90 and TOM70 used specific peptides from these proteins in a competition inhibition assay involving protein translocation by the Hsp90-TOM70 system [9]. One of the peptides, Hsp90-GYSRMEEVD, contains the canonical MEEVD Hsp90 motif that binds to TPR, corresponding to approximately 40% translocation inhibition [9]. Other peptides, Hsp90-TLRQKAEADKNDKSVKDLVILLY and Tom70-LLADKVLKLLGKEKAKEKY (magenta in Fig. 1B), which correspond to a second site of interaction between Hsp90 and TOM70, inhibit translocation by approximately 40 and 35%, respectively [9]. Additionally, the combination of the two Hsp90 peptides, representing the two sites, results in a translocation inhibitory level similar to that of a competition inhibition assay by adding the
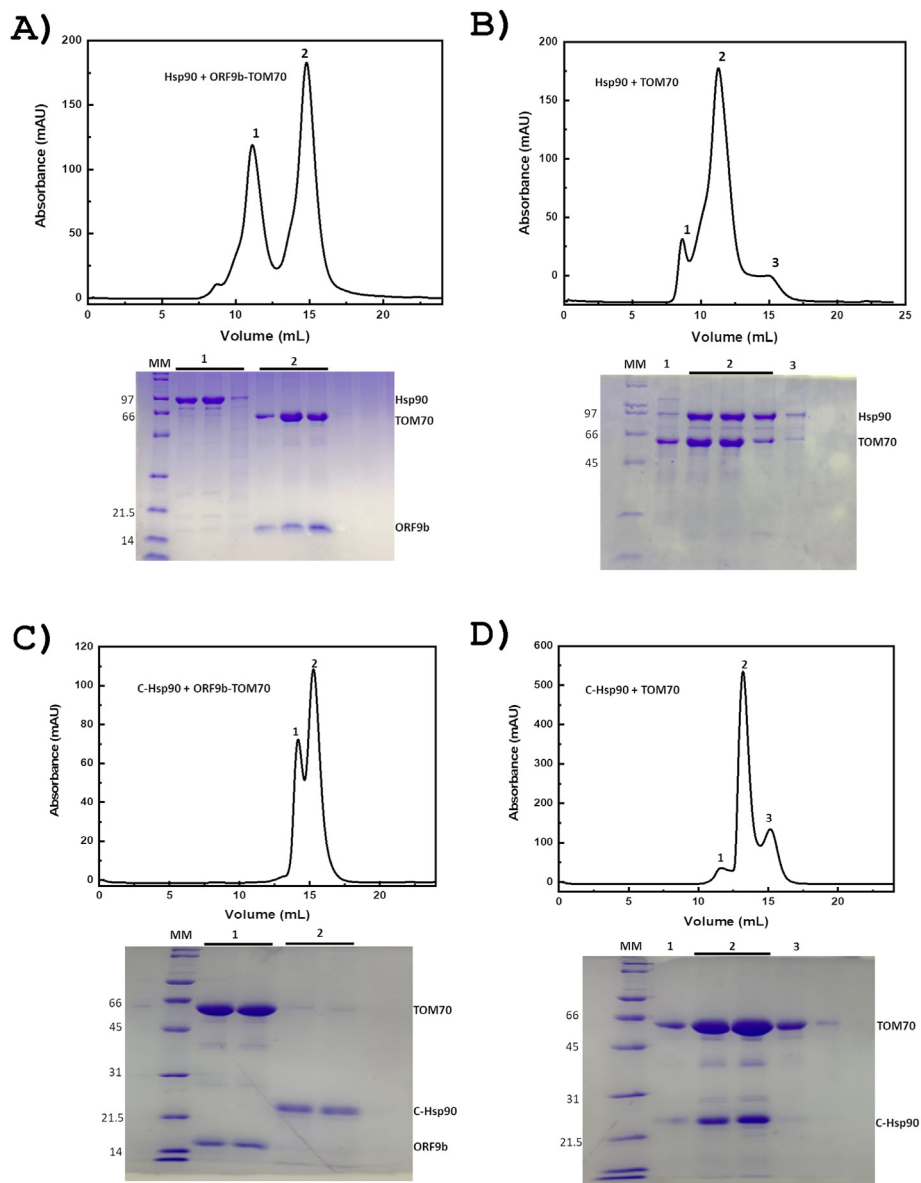
Fig. 5. Protein−protein interaction by analytical gel filtration and SEC-MALS. A) Analytical gel filtration (GF) chromatogram of 50 μM Hsp90 and 25 μM ORF9b-TOM70. The chromatogram shows two peaks of unbound proteins whose fractions were analyzed by SDS−PAGE, as shown below, corresponding to the Hsp90 and ORF9b-TOM70 complexes. **B)** Analytical GF chromatogram of 50 μM Hsp90 and 25 μM TOM70, which shows one major peak (peak two). Fractions were analyzed by SDS−PAGE corresponding to a complex formation of Hsp90 and TOM70. Other minor peaks (peaks 1 and 3) show subcomplexes containing partial assemblies. **C)** Analytical GF chromatogram of 50 μM C-Hsp90 (C-terminal domain) and 25 μM ORF9b-TOM70 shows two peaks of unbound proteins whose fractions were analyzed by SDS−PAGE shown below, corresponding to the C-Hsp90 and ORF9b-TOM70 complexes. **D)** Analytical GF chromatogram of 50 μM C-Hsp90 and 25 μM TOM70 alone shows one major peak (peak two) whose fractions were analyzed by SDS−PAGE shown below, corresponding to a complex formation of C-Hsp90 and TOM70. Other minor peaks (peaks 1 and 3) show subcomplexes containing partial assemblies.

entire Hsp90 protein [9]. These results clearly indicate that, together, the two sites account for the strength of the whole interaction and that each contributes equally to the Hsp90-TOM70 interaction. Gao and colleagues [11] argued that occupation of ORF9b at the C-terminal of TOM70 may severely disrupt binding of the MEEVD motif at the N-terminus. We suggest that our findings add important additional information to their model to generate a more detailed one. Therefore, we need to consider the crystal structure of the ORF9b-TOM70 complex (PDB: 7DHG) to highlight the interaction sites (Fig. 6A−B), in which we mapped the following binding regions on TOM70: 1) in blue, the ORF9b interacting residues E549, H583, E477, Q379, Q381, D545, H515, Q594, and V556 and the residue E580 seen by cryo-EM structure (7KDT). 2), in yellow, the residues that interact with the MEEVD motif of Hsp90,

adapted from the crystal structure of yeast TOM71 in complex with the Hsp82 C-terminal fragment (PDB: 3FP2) [13]. 3), in cyan, Trp residues. 4), in magenta, the identified second functional interaction site with Hsp90, which includes the sequence LLADKVLKLLG-KEKAKEKY located on helix α7 ([9]; Fig. 6).

A direct indication that the second binding site in TOM70, the first site being the one binding the MEEVD motif, is involved in the inhibition process emerged from the observation that this region (helix α7; Fig. 6) is in close proximity to the residues H583, E580, Q379 and Q381 (Fig. 6, in blue), i.e., the binding region of ORF9b. Therefore, binding of ORF9b to TOM70 is likely to perturb the conformational position of helix α7, which contains the second site of interaction with Hsp90. This hypothesis is strongly supported by the superimposition of the crystal structures of TOM70 bound to
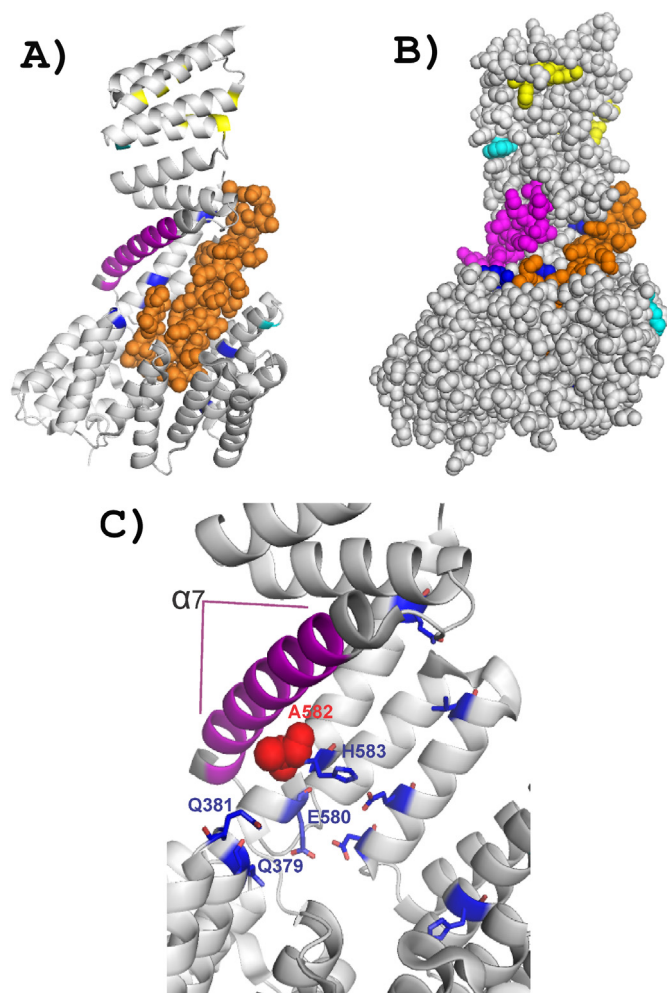
Fig. 6. TOM70 structural arrangement and regions of interaction. (**A**) Crystal structure of the ORF9b-TOM70 complex (PDB: 7DHG). Helices of TOM70 and all residues of ORF9b. Residues marked in yellow show the TPR domain that interacts with the MEEVD motif of Hsp90, adapted from the crystal structure of yeast TOM71 in complex with the Hsp82 C-terminal fragment (PDB: 3FP2). Magenta shows the region (located on helix α7) from the newly identified second functional interaction site with Hsp90. Blue shows the ORF9b interacting residues on TOM70, which include residues E549, H583, E477, Q379, Q381, D545, H515, Q594, V556, and E580. Cyan, Trp residues. **B**) Surface model of the crystal structure of the ORF9b-TOM70 complex (see A) for details. **C**) Closer view of helix α7 (second site of interaction with Hsp90) and residues H583, E580, Q379, and Q381 at the binding region of ORF9b. Highlight of residue Ala582 (red) that is in close contact with helix α7 (magenta), in which lies the second site of interaction with Hsp90), and is found mutated in a disease caused by poor translocation of key proteins to mitochondria (see text).

ORF9b with that of free TOM71, which indicates structural rearrangements on helices α7 and α8 upon binding [11]. In fact, the superimposition shows that the region comprising helices α7 and α8 is stabilized by the binding of ORF9b [11]. Therefore, a model materializes in which the binding of ORF9b to TOM70 perturbs not only the region that binds the Hsp90 MEEVD motif but also the region of helix α7, which lies at the second site of interaction with Hsp90. Another support to this model involves the results from Trp fluorescence. Trp residues (cyan in Fig. 6A–B), contrary to helix α7, are not near the binding site and thus are not perturbed by it and do not change their emitted fluorescence upon binding (Fig. 3B). Additional support to our model emerges from recent evidence that a mutation in the residue Ala582 to Val in human TOM70 is related to an anemia condition in patients that is caused by poor translocation of key proteins to the mitochondria [27]. This residue is at

the bottom of helix α7 (magenta, Fig. 6C), in which lies the second site of interaction with Hsp90, and in close proximity to those (in blue) responsible for binding ORF9b. Valine has a side-chain with a volume about three times bigger than that of Alanine and the mutation is likely to cause a rearrangement of helix α7 to accommodate the packing of the extra volume, eliminating Hsp90 binding and resulting in poor protein translocation as detected in anemic patients [27]. That is, perturbations in the residues located at this region (i.e. A582 or those binding ORF9b; Fig. 6C), which is near the helix α7, inhibit the interaction between TOM70 and Hsp90 by affecting their second site of interaction.

In conclusion, the combination of the results shown in this work with those previously published [9,11,27] give support to our model and suggest that ORF9b binding is very efficient in inhibiting Hsp90 and thus evading the immune response because it targets not one but two sites of interaction between TOM70 and Hsp90. The fact that the two sites are equally efficient in the binding process between Hsp90 and TOM70 [9] highlights the effectiveness of the inhibitory effect caused by ORF9b. This finding is relevant because the ORF9b-TOM70 interaction is an attractive target for the development of therapeutic strategies in COVID-19 infection since it has been previously shown that TOM70 is involved in a signaling cascade that ultimately leads to the induction of type I interferons (IFN–I). SARS-CoV-2 can evade host immunity through the downregulation of IFN production in the host cell [4,5,28]. This cascade depends on the recruitment of Hsp90-bound proteins to the N-terminal domain of TOM70, thus recruiting TBK1/IRF3 to mitochondria, and disruption of this interaction impairs the activation of TBK1 and IRF3, which are critical steps to the mitochondrial antiviral system and induction of type I interferons (IFN–I) [10,29]. Therefore, our results and analyses provide several lines of evidence that support the findings that inhibition of Hsp90 binding to TOM70 by ORF9b is the reason for the reduced IFN-I and overall host immune evasion of SAR-CoV-2 [30].

4. Conclusion

This work was developed with the aim of adding relevant information on the mechanism by which SARS-CoV-2 ORF9b inhibits the interaction between Hsp90 and TOM70, allowing the virus to evade the immune response at the end of the line. The three mentioned proteins and the C-terminal domain of Hsp90 were produced and purified. ORF9b alone was produced partially folded as a dimer in solution, and the conformation of the other studied proteins has been characterized previously [7,9,16]. Coexpression of ORF9b with TOM70 resulted in a folded heterodimer that was more stable than TOM70 alone and was the main object of investigation.

A combination of protein–protein interaction assays showed that both the full-length and the C-terminal domain of Hsp90 were able to bind to TOM70 alone but not to the ORF9b-TOM70 complex, confirming the basis for immune evasion by SARS-CoV-2. We argued that the combination of the results shown in this work with those previously published [9,11] provides strong support for a model for the inhibitory action of ORF9b. This model mainly includes the following: 1) neither full-length Hsp90 nor its C-terminal domain binds ORF9b-TOM70 complex; 2) Hsp90 contains two TOM70 binding sites in its C-terminal domain, one is the MEEVD motif and the other is a recently found second site; 3) the second site TOM70-peptide contributes to approximately half of the interaction strength between TOM70 and Hsp90, measured in a competitive inhibitory assay, and corresponds to helix α7; and 4) helices α7 and α8 of TOM70 experience structural rearrangement upon ORF9b binding. Thus, the binding of ORF9b to TOM70 perturbs not only the region that binds the Hsp90 MEEVD motif but also the region of helix α7, which lies at the second site of

interaction with Hsp90, supporting a more detailed model for the inhibition caused by ORF9b (see Graphical Abstract). In conclusion, the findings presented are relevant because the ORF9b-TOM70 interaction is an attractive target for the development of therapeutic strategies against COVID-19 infection.

Authors contribution

A.K.S. and G.M.S.P.: collection of data and analysis of data. C.H.I.R. conception of the work, collection of data and analysis of data. All authors: drafted, critically reviewed and approved the final article.

Declaration of competing interest

The authors declare no competing interests.

Acknowledgements

References

[1] B. Hu, H. Guo, P. Zhou, Z.L. Shi, Characteristics of SARS-CoV-2 and COVID-19, Nat. Rev. Microbiol. 19 (2021) 141–154, https://doi.org/10.1038/s41579-020-00459-7.

[2] N. Kirtipal, S. Bharadwaj, S.G. Kang, From SARS to SARS-CoV-2, insights on structure, pathogenicity and immunity aspects of pandemic human coronaviruses, Infect. Genet. Evol. : journal of molecular epidemiology and evolutionary genetics in infectious diseases 85 (2020), https://doi.org/10.1016/j.meegid.2020.104502, 104502-104502.

[3] S. Wang, T. Dai, Z. Qin, T. Pan, F. Chu, L. Lou, L. Zhang, B. Yang, H. Huang, H. Lu, et al., Targeting liquid-liquid phase separation of SARS-CoV-2 nucleocapsid protein promotes innate antiviral immunity by elevating MAVS activity, Nat. Cell Biol. 23 (2021) 718–732, https://doi.org/10.1038/s41556-021-00710-0.

[4] L. Han, M.-W. Zhuang, J. Deng, Y. Zheng, J. Zhang, M.-L. Nan, X.-J. Zhang, C. Gao, P.-H. Wang, SARS-CoV-2 ORF9b antagonizes type I and III interferons by targeting multiple components of the RIG-I/MDA-5-MAVS, TLR3-TRIF, and cGAS-STING signaling pathways, J. Med. Virol. 93 (2021) 5376–5389, https://doi.org/10.1002/jmv.27050.

[5] H.W. Jiang, H.N. Zhang, Q.F. Meng, J. Xie, Y. Li, H. Chen, Y.X. Zheng, X.N. Wang, H. Qi, J. Zhang, et al., SARS-CoV-2 Orf9b suppresses type I interferon responses by targeting TOM70, Cell. Mol. Immunol. 17 (2020) 998–1000, https://doi.org/10.1038/s41423-020-0514-8.

[6] N. Redondo, S. Zaldívar-López, J.J. Garrido, M. Montoya, SARS-CoV-2 accessory proteins in viral pathogenesis: knowns and unknowns, Front. Immunol. 12 (2021), 708264, https://doi.org/10.3389/fimmu.2021.708264.

[7] L.M. Gava, D.C. Gonçalves, J.C. Borges, C.H. Ramos, Stoichiometry and thermodynamics of the interaction between the C-terminus of human 90kDa heat shock protein Hsp90 and the mitochondrial translocase of outer membrane Tom70, Arch. Biochem. Biophys. 513 (2011) 119–125, https://doi.org/10.1016/j.abb.2011.06.015.

[8] J.C. Young, N.J. Hoogenraad, F.U. Hartl, Molecular chaperones Hsp90 and Hsp70 deliver preproteins to the mitochondrial import receptor Tom70, Cell 112 (2003) 41–50, https://doi.org/10.1016/s0092-8674(02)01250-3.

[9] L.M. Zanphorlin, T.B. Lima, M.J. Wong, T.S. Balbuena, C.A. Minetti, D.P. Remeta, J.C. Young, L.R. Barbosa, F.C. Gozzo, C.H. Ramos, Heat shock protein 90 kDa (Hsp90) has a second functional interaction site with the mitochondrial import receptor Tom70, J. Biol. Chem. 291 (2016) 18620–18631, https://doi.org/10.1074/jbc.M115.710137.

[10] X.Y. Liu, B. Wei, H.X. Shi, Y.F. Shan, C. Wang, Tom70 mediates activation of interferon regulatory factor 3 on mitochondria, Cell Res. 20 (2010) 994–1011, https://doi.org/10.1038/cr.2010.103.

[11] X. Gao, K. Zhu, B. Qin, V. Olieric, M. Wang, S. Cui, Crystal structure of SARS-CoV-2 Orf9b in complex with human TOM70 suggests unusual virus-host interactions, Nat. Commun. 12 (2021) 2843, https://doi.org/10.1038/s41467-021-23118-8.

[12] D.E. Gordon, J. Hiatt, M. Bouhaddou, V.V. Rezelj, S. Ulferts, H. Braberg, A.S. Jureka, K. Obernier, J.Z. Guo, J. Batra, et al., Comparative host-coronavirus protein interaction networks reveal pan-viral disease mechanisms, Science (2020) 370, https://doi.org/10.1126/science.abe9403.

[13] J. Li, X. Qian, J. Hu, B. Sha, Molecular chaperone Hsp70/Hsp90 prepares the mitochondrial outer membrane translocon receptor Tom71 for preprotein loading, J. Biol. Chem. 284 (2009) 23852–23859, https://doi.org/10.1074/jbc.M109.023986.

[14] C. Scheufler, A. Brinker, G. Bourenkov, S. Pegoraro, L. Moroder, H. Bartunik, F.U. Hartl, I. Moarefi, Structure of TPR domain-peptide complexes: critical elements in the assembly of the Hsp70-Hsp90 multichaperone machine, Cell 101 (2000) 199–210, https://doi.org/10.1016/s0092-8674(00)80830-2.

[15] H. Edelhoch, Spectroscopic determination of tryptophan and tyrosine in proteins, Biochemistry 6 (1967) 1948–1954, https://doi.org/10.1021/bi00859a010.

[16] L.M. Zanphorlin, F.R. Alves, C.H. Ramos, The effect of celastrol, a triterpene with antitumorigenic activity, on conformational and functional aspects of the human 90kDa heat shock protein Hsp90α, a chaperone implicated in the stabilization of the tumor phenotype, Biochim. Biophys. Acta 1840 (2014) 3145–3152, https://doi.org/10.1016/j.bbagen.2014.06.008.

[17] D.H. Correa, C.H. Ramos, The use of circular dichroism spectroscopy to study protein folding, form and function, Afr. J. Biochem. Res. 3 (2009) 164–173, https://doi.org/10.5897/AJBR.9000245.

[18] D. Some, H. Amartely, A. Tsadok, M. Lebendiker, Characterization of proteins by size-exclusion chromatography coupled to multi-angle light scattering (SEC-MALS), J Vis Exp (2019), https://doi.org/10.3791/59615.

[19] S. Kreimendahl, J. Rassow, The mitochondrial outer membrane protein tom70-mediator in protein traffic, membrane contact sites and innate immunity, Int. J. Mol. Sci. 21 (2020), https://doi.org/10.3390/ijms21197262.

[20] F.A. Batista, L.M. Gava, G.M. Pinheiro, C.H. Ramos, J.C. Borges, From conformation to interaction: techniques to explore the Hsp70/Hsp90 network, Curr. Protein Pept. Sci. 16 (2015) 735–753, https://doi.org/10.2174/1389203716666150505225744.

[21] L.L. Porter, Predictable fold switching by the SARS-CoV-2 protein ORF9b, Protein Sci. 30 (2021) 1723–1729, https://doi.org/10.1002/pro.4097.

[22] J.D. Morrisett, J.S. David, H.J. Pownall, A.M. Gotto Jr., Interaction of an apolipoprotein (apoLP-alanine) with phosphatidylcholine, Biochemistry 12 (1973) 1290–1299, https://doi.org/10.1021/bi00731a008.

[23] N. Greenfield, G.D. Fasman, Computed circular dichroism spectra for the evaluation of protein conformation, Biochemistry 8 (1969) 4108–4116, https://doi.org/10.1021/bi00838a031.

[24] N. Hellmann, D. Schneider, Hands on: using tryptophan fluorescence spectroscopy to study protein structure, Methods Mol. Biol. 1958 (2019) 379–401, https://doi.org/10.1007/978-1-4939-9161-7_20.

[25] C.H. Ramos, S.T. Ferreira, Protein folding, misfolding and aggregation: evolving concepts and conformational diseases, Protein Pept. Lett. 12 (2005) 213–222, https://doi.org/10.2174/0929866053587156.

[26] A.C. Fan, M.K. Bhangoo, J.C. Young, Hsp90 functions in the targeting and outer membrane translocation steps of Tom70-mediated mitochondrial import, J. Biol. Chem. 281 (2006) 33313–33324, https://doi.org/10.1074/jbc.M605250200.

[27] X. Wei, M. Du, J. Xie, T. Luo, Y. Zhou, K. Zhang, J. Li, D. Chen, P. Xu, M. Jia, et al., Mutations in TOMM70 lead to multi-OXPHOS deficiencies and cause severe anemia, lactic acidosis, and developmental delay, J. Hum. Genet. 65 (2020) 231–240, https://doi.org/10.1038/s10038-019-0714-1.

[28] D. Blanco-Melo, B.E. Nilsson-Payant, W.C. Liu, S. Uhl, D. Hoagland, R. Møller, T.X. Jordan, K. Oishi, M. Panis, D. Sachs, et al., Imbalanced host response to SARS-CoV-2 drives development of COVID-19, Cell 181 (2020) 1036–1045, https://doi.org/10.1016/j.cell.2020.04.026, e1039.

[29] B. Wei, Y. Cui, Y. Huang, H. Liu, L. Li, M. Li, K.C. Ruan, Q. Zhou, C. Wang, Tom70 mediates Sendai virus-induced apoptosis on mitochondria, J. Virol. 89 (2015) 3804–3818, https://doi.org/10.1128/jvi.02959-14.

[30] L. Brandherm, A.M. Kobaš, M. Klöhn, Y. Brüggemann, S. Pfaender, J. Rassow, S. Kreimendahl, Phosphorylation of SARS-CoV-2 Orf9b regulates its targeting to two binding sites in TOM70 and recruitment of Hsp90, Int. J. Mol. Sci. 22 (2021), https://doi.org/10.3390/ijms22179233.